

Article

Phosphorus Containing Polyacrylamides as Flame Retardants for Epoxy-Based Composites in Aviation

Lara Greiner ¹, Philipp Kukla ¹, Sebastian Eibl ² and Manfred Döring ^{1,*} 

- ¹ Fraunhofer Institute for Structural Durability and System Reliability LBF, Schlossgartenstr. 6, 64289 Darmstadt, Germany; lara.greiner@lbf.fraunhofer.de (L.G.); philipp.kukla@lbf.fraunhofer.de (P.K.)
- ² Bundeswehr Research Institute for Materials, Fuels and Lubricants, Institutsweg 1, 85435 Erding, Germany; SebastianEibl@bundeswehr.org
- * Correspondence: manfred.doering@lbf.fraunhofer.de; Tel.: +49-6151-705-8675

Received: 21 January 2019; Accepted: 4 February 2019; Published: 8 February 2019



Abstract: Novel polymeric flame retardants based on two acrylamides and 9,10-dihydro-9-oxa-10-phosphaphenanthrene-10-oxide (DOPO) or 5,5-dimethyl-[1,3,2]dioxaphosphinane-2-oxide (DDPO) are described for several applications in HexFlow[®] RTM6, a high-performance epoxy resin. Neat resin samples and carbon fiber-reinforced composites were tested for their glass transition temperatures (dynamic mechanical analysis), thermal stability (thermogravimetric analyses), flammability (UL94) and flame-retardant performance (Cone Calorimetry). Additionally, the fiber degradation occurring during combustion of carbon fiber-reinforced epoxy resins was observed by scanning electron microscopy to show the fiber protecting effect of these flame retardants. Whereas DOPO-containing polyacrylamides acting mainly in the gas phase showed the best flame retardant efficiency, DDPO-containing polyacrylamides acting mainly in the condensed phase showed the best fiber protection. A mixed polyacrylamide was synthesized to combine these effects. This thermoplastic is soluble in the resin and, therefore, suitable for injection molding processes. Interlaminar shear strength measurements showed no negative effect of the flame retardant. The versatility of these flame retardants is shown by investigations dealing with boehmite as synergist in neat resin samples.

Keywords: epoxy resin; composite; fiber degradation; phosphorus-containing flame retardants

1. Introduction

Epoxy-based composites can be found in numerous highly sophisticated aerospace applications. In particular, carbon fiber reinforcement leads to lightweight materials with optimized mechanical properties. For many applications, adjusted flame retardancy is necessary. The efficiency of incorporated flame retardants depends on the epoxy resin matrix and the reinforcement [1–10].

Moreover, it is well known that carbon fibers can form respirable fiber fragments after a thermal load and fire [11,12]. Several aircraft crashes accompanied by fire have increased the interest in assessing the additional health risk of respirable carbon fiber dust. Critical fiber concentrations were reported for large-scale fire tests and collecting the flight recorder of a crashed helicopter [13,14]. Carbon fibers consist of more than 90% carbon (typically over 95%) with a residue of mainly nitrogen, which makes them prone to oxidation reactions. Within minutes a significant oxidation reaction is observed above 600 °C in air. This reaction is influenced by heating rate and strongly influenced by oxygen concentration [15]. A continuous decrease of fiber diameter and a formation of surface defects, which end up in a pronounced hole structure at severe damage, have been observed. After 10 min at 650 °C, fibers thinner than 3 µm were detected [15]. According to the definition of the World Health Organization (WHO), fibers thinner than 3 µm longer than 5 µm are considered to be respirable. Additionally, the length to diameter ratio has to be higher than 3. Fibers with these

dimensions are thin enough to penetrate the deep lung areas (alveoli), and too long to be exhaled [16]. As long as carbon fiber-reinforced thermoset polymers (CFRP) are not exposed to high temperatures or other degradation processes, commercially available carbon fibers are typically thicker than 5 μm and, therefore, uncritical with regard to inhalation. Consequently there is a need for fiber protection in addition to flame retardancy. With respect to fiber-matrix adhesion, literature [15,17] showed that the addition of zinc borate shows fiber protection by the formation of a glassy surface layer on the fibers during matrix combustion. However, zinc borate is not suitable for resin transfer molding, an important process for the manufacturing of fiber-reinforced epoxy based composites. It increases the viscosity of the resin significantly and the inhomogeneously dispersed particles are filtered by the fiber plies during injection.

Widely discussed flame retardants for epoxy resins and composites thereof are phosphorus containing compounds. For phosphorus containing flame retardants, the mode of action depends on the phosphorus species and the polymer they are incorporated [18,19]. If the chemical environment of the phosphorus is carbon/hydrogen rich, it promotes action in the gas phase. An oxygen rich environment promotes action in the condensed phase, respectively. Moreover, a trend to polymeric, oligomeric or star-shaped flame retardants is observed to avoid leaching and to ensure the high mechanical and thermal requirements of the composites [1,2,9,20–26]. Investigations with triazines [27] or phosphazenes [28] showed the synergistic effects of phosphorus and nitrogen containing units.

To combine different phosphorus species in polymeric or oligomeric nitrogen-containing molecules, a new approach is investigated. Oligomeric flame retardants were synthesized by Phospha-Michael addition of phosphorus compounds like the carbon rich 9,10-dihydro-9-oxa-10-phosphaphenanthrene-10-oxide (DOPO) or the oxygen rich 5,5-dimethyl-1,3,2-dioxaphosphorinan-2-one (DDPO) and multifunctional acrylamides with the following radical polymerization of residual double bonds (Figure 1). Dependent on the acrylamide used (e.g. *N,N'*-methylenebisacrylamide (BA) or 1,3,5-triacryloylhexahydro-1,3,5-triazine (TAHHT)) and the ratio of phosphorus containing molecules to double bonds, oligomeric or polymeric products with either thermoset or thermoplastic properties are formed. Whereas DOPO, which is more likely to act in the gas-phase, shall provide mainly flame retardancy for carbon fiber-reinforced epoxy resins, DDPO may initiate the formation a protective layer on the carbon fibers to retard the formation of respirable carbon fiber fragments. This work compares flame retardant properties and fiber protection of BA-DOPO, TAHHT-DOPO and TAHHT-DOPO-DDPO with thermoplastic properties and TAHHT-DDPO with thermoset properties. Due to the lower reactivity of the P-H-group in DDPO, the conversion of double bonds by Phospha-Michael addition was not sufficient to yield a thermoplastic compound.

The following work includes an additional possible application for the novel flame retardants in a prepreg system matrix. Aluminum hydroxides, especially aluminum tri-hydroxide (ATH), are often used as flame retardant inorganic fillers. Due to low flame retardant efficiencies, high loadings of the hydroxides are required and have a negative effect on mechanical properties and processability [29]. Therefore, the filler loading is reduced by addition of synergistic flame retardants like phosphorus-based compounds [30,31]. For epoxy resins, there are known synergists in combination with ATH. Boehmite is an inorganic filler used for temperatures up to 300 °C. The synergistic effect of boehmite together with DOPO is described in the literature for epoxy resins like bisphenol A diglycidyl ether hardened with dicyandiamide and fenuron [30]. A lower surface area of boehmite results in more flame retardant species in combination with phosphinates [3].

These investigations show the synergistic effect of the novel phosphorus containing polyacrylamides and two different types of boehmite in a high-performance epoxy resin.

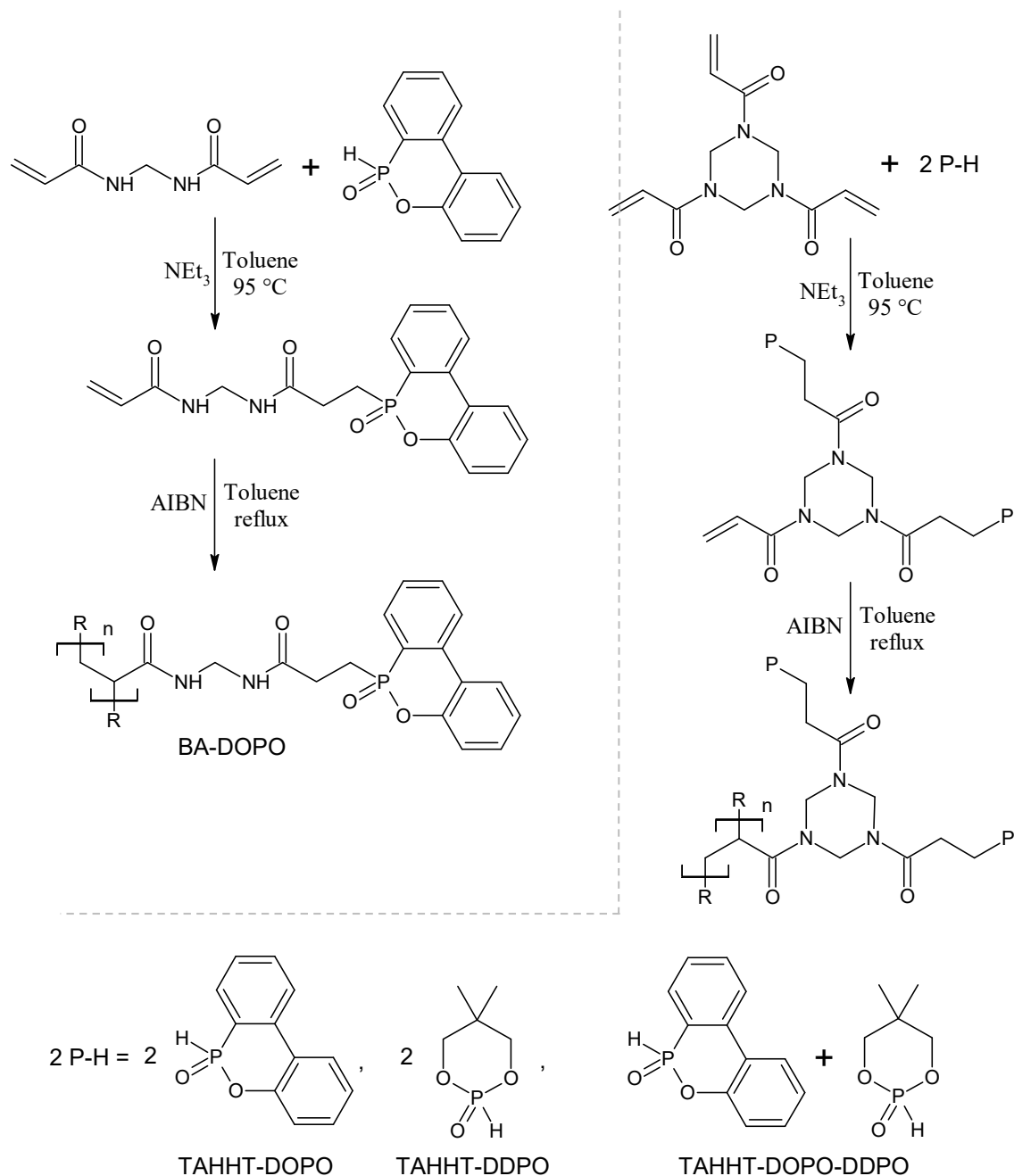


Figure 1. Synthesis of BA-DOPO, TAHHT-DOPO, TAHHT-DDPO and TAHHT-DOPO-DDPO. Detailed ratios are shown in the synthesis descriptions.

2. Materials and Methods

Unless stated otherwise, solvents and chemicals were obtained from commercial sources and used as received.

2.1. Synthesis of BA-DOPO

Into a 1 L three-necked round bottom flask equipped with a thermometer, a reflux condenser with a drying tube (sodium hydroxide filled) and a sealed precision glass stirrer 600 mL toluene, 18 mL (130 mmol) triethylamine (anhydrous), 200 mg 4-methoxyphenol and 50.0 g (324 mmol, 1.00 eq.) *N,N'*-methylenebisacrylamide were introduced. The mixture was heated to 95 °C while stirring and under vigorous stirring, 73.5 g (340 mmol, 1.05 eq.) DOPO was added in small portions within 3 h.

After continuing stirring at 95 °C for additional 25 h, the full conversion of DOPO was observed by ³¹P-nuclear magnetic resonance (NMR) (CDCl₃, 300 MHz, 298 K, NanoBay 300, Bruker, Billerica, MA, USA): 37.64 ppm (m). The drying tube was exchanged with a nitrogen inlet and the apparatus was filled with nitrogen. The mixture was refluxed for 1 h. Afterwards, 1.5 mL of 2,2'-azobis(2-methylpropionitrile) (AIBN) solved in toluene (0.2 mol·L⁻¹) was added. After 5 min another 0.5 mL of this solution was added. The mixture was refluxed for additional 3 h during which a viscous oligomer precipitated. After cooling down to about 60 °C, the solution was filtered and the product was washed with toluene. Drying in vacuo at 90 °C for 24 h resulted in a white powder. The yield was 118 g (96%). ³¹P-NMR (CDCl₃, 300 MHz, 298 K): 37.25 ppm (m); ¹H-NMR (CDCl₃, 300 MHz, 298 K): 7.92 ppm (NH, m, 1H), 7.89 ppm (NH, m, 1H) 7.69 ppm (CH_{arom}, m, 1H), 7.50 ppm (CH_{arom}, m, 1H), 7.36 ppm (CH_{arom}, m, 1H), 7.18 ppm (CH_{arom}, m, 4H), 6.96 ppm (CH_{arom}, m, 1H), 4.63 ppm + 4.51 ppm (CH₂, t, ³J_{HH} 6.12 Hz + 5.77 Hz, 2H), 2.49 ppm + 2.39 ppm (CH_{Backbone}/CH₂, m/s, 7H).

2.2. Synthesis of TAHHT-DOPO

Into a 1 L three-necked round bottom flask equipped with a thermometer, a reflux condenser with a drying tube (sodium hydroxide filled) and a sealed precision glass stirrer 400 mL toluene, 12 mL (87 mmol) triethylamine (anhydrous), 200 mg 4-methoxyphenol and 30.0 g (120 mmol, 1.00 eq.) 1,3,5-triacryloylhexahydro-1,3,5-triazine were introduced. The mixture was heated to 95 °C while stirring and under vigorous stirring, 54.4 g (252 mmol, 2.10 eq.) DOPO was added in small portions within 3 h. After continuing stirring at 95 °C for additional 15 h, the full conversion of DOPO was observed by ³¹P-NMR (CDCl₃, 300 MHz, 298 K): 37.34 ppm (m). The drying tube was exchanged by a nitrogen inlet and the apparatus was filled with nitrogen. The mixture was refluxed for 2 h. Afterwards 1.2 mL of 2,2'-azobis(2-methylpropionitrile) solved in toluene (0.2 mol·L⁻¹) was added. After 5 min another 1.0 mL of this solution were added. The mixture was refluxed for additional 3 h during which a viscous oligomer precipitated. After cooling down to about 60 °C, the solution was filtered and the product was washed with toluene. Drying in vacuo at 130 °C for 12 h resulted in a white powder. The yield was 83 g (98%). ³¹P-NMR (CDCl₃, 300 MHz, 298 K): 37.27 ppm (m); ¹H-NMR (CDCl₃, 300 MHz, 298 K): 7.89 ppm (CH_{arom}, m, 4H), 7.64 ppm (CH_{arom}, m, 2H), 7.46 ppm (CH_{arom}, m, 2H), 7.18 ppm (CH_{arom}, m, 8H), 5.19 ppm (C_{aliph}, m, 6H), 2.84 ppm (C_{Backbone}, m, 3H), 2.35 ppm (C_{aliph}, s, 8H).

2.3. Synthesis of TAHHT-DDPO

Into a 1 L three-necked round bottom flask equipped with a thermometer, a reflux condenser with a drying tube (sodium hydroxide filled) and a sealed precision glass stirrer 400 mL toluene, 12 mL (87 mmol) triethylamine (anhydrous), 200 mg 4-methoxyphenol and 30.0 g (120 mmol, 1.00 eq.) 1,3,5-triacryloylhexahydro-1,3,5-triazine were introduced. The mixture was heated to 95 °C while stirring and under vigorous stirring, 32.0 g (216 mmol, 1.80 eq.) DDPO was added in small portions within 3 h. After continuing stirring at 95 °C for additional 15 h, the full conversion of DDPO was observed by ³¹P-NMR (CDCl₃, 300 MHz, 298 K): 27.38 ppm (m). The drying tube was exchanged by a nitrogen inlet and the apparatus was filled with nitrogen. The mixture was refluxed for 2 h. Afterwards 1.2 mL of 2,2'-azobis(2-methylpropionitrile) solved in toluene (0.2 mol·L⁻¹) was added. After 5 min another 1.0 mL of this solution were added. The mixture was refluxed for additional 3 h during which a viscous oligomer precipitated. After cooling down to about 60 °C, the solution was filtered and the product was washed with toluene. Drying in vacuo at 110 °C for 15 h resulted in a white insoluble powder with thermoset properties. The yield was 57 g (92%).

2.4. Synthesis of TAHHT-DOPO-DDPO

Into a 1 L three-necked round bottom flask equipped with a thermometer, a reflux condenser with a drying tube (sodium hydroxide filled) and a sealed precision glass stirrer 400 mL toluene, 12 mL (87 mmol) triethylamine (anhydrous), 200 mg 4-methoxyphenol and 30.0 g (120 mmol, 1.00 eq.) 1,3,5-triacryloylhexahydro-1,3,5-triazine were introduced. The mixture was heated to 95 °C while

stirring and under vigorous stirring, 17.8 g (120 mmol, 1.00 eq.) DDPO was added in small portions within 3 h. After continuing stirring at 95 °C for 25 h, 28.5 g (132 mmol, 1.10 eq) DOPO were added in small portions within 2 h. After another 10 h at 95 °C, the full conversion of DOPO and DDPO was observed by ^{31}P -NMR (CDCl_3 , 300 MHz, 298 K): 27.44 ppm (m), 37,29 ppm (s). The drying tube was exchanged by a nitrogen inlet and the apparatus was filled with nitrogen. The mixture was refluxed for 2 h. Afterwards 1.2 mL of 2,2'-azobis(2-methylpropionitrile) solved in toluene ($0.2 \text{ mol}\cdot\text{L}^{-1}$) was added. After 5 min, another 1.0 mL of this solution were added. The mixture was refluxed for additional 3 h during which a viscous oligomer precipitated. After cooling down to about 60 °C, the solution was filtered and the product was washed with toluene. Drying in vacuo at 110 °C for 15 h resulted in a white powder. The yield was 74 g (97%). ^{31}P -NMR (CDCl_3 , 300 MHz, 298 K): 27.33 ppm (m, DDPO, 0.45 equivalent), 37.31 ppm (s, DOPO, 0.55 equivalent).

2.5. Characterization

Pure flame retardants were analyzed by thermogravimetric analyses (TGA; Q500, TA Instruments, Inc., New Castle, DE, USA) starting at room temperature and heated to 800 °C under nitrogen or synthetic air (50 ml/min) with a heating rate of $10 \text{ K}\cdot\text{min}^{-1}$.

Reaction-to-fire tests were performed with the carbon fiber reinforced system HexFlow[®] RTM6 (aromatic epoxy resin matrix) and HexForce[®] G0939 (carbon fiber fabric) from Hexcel Composites GmbH (Stade, Germany) [32]. The matrix was modified by amounts of 10% by matrix weight of BA-DOPO, TAHHT-DOPO, TAHHT-DDPO or TAHHT-DOPO-DDPO. Mixing was carried out at 120 °C for 15 min. Eight plies were laminated by hand, resulting in 2 mm thick lay-ups: [(0|90)]₈. This procedure is described in the literature [33]. The specimens were cured in an autoclave according to the manufacturer's recommended conditions [32]. The cured laminates were cut into specimens of $100 \times 100 \text{ mm}$ for cone calorimetric measurements and specimens of $20 \times 10 \text{ mm}$ for the measurement of the interlaminar shear strength with a water-cooled diamond wheel saw. Additionally, samples of flame retarded RTM6 without fiber reinforcement were prepared (2 mm, 4 mm). Curing of these samples was carried out with the same temperature program as the composites but under atmospheric pressure. Specimens of $30 \times 10 \times 2 \text{ mm}$ for dynamic mechanical analysis, $70 \times 13 \text{ mm} \times 4 \text{ mm}$ for UL94-tests were trimmed with a band-saw.

Synergism with boehmite was tested with synthetic boehmite Actilox[®] B30 (Nabaltec AG, Schwandorf, Germany) and Disperal[®] 40 (Sasol Germany GmbH, Brunsbüttel, Germany). Actilox[®] B30 is a high purity boehmite (99%) with a particle size D_{50} of 1.8 μm and specific surface area (BET) of $3 \text{ m}^2\cdot\text{g}^{-1}$. Disperal[®] 40 is an acid dispersible boehmite with lower purity (94%) and bigger particles (35 μm) with higher BET-surface ($100 \text{ m}^2\cdot\text{g}^{-1}$). Neat resin samples were prepared as described above for 35% boehmite and 30% boehmite in combination with 5% TAHHT-DDPO or TAHHT-DOPO.

An overview of the prepared samples is given in Table 1.

Specimens 4 mm thick were analyzed by UL-94 (Dr.-Ing. Georg Wazau Mess- + Prüfsysteme GmbH, Berlin, Germany) according to DIN EN 60695-11-10 [34] and 2 mm thick specimens were investigated by dynamic mechanical analysis (DMA; SEIKO SII EXSTAR 6100 DMS, Seiko Instruments Inc., Chiba, Japan) with single cantilever geometry from 35 °C to 260 °C with a frequency of 1 Hz and a heating rate of $3 \text{ K}\cdot\text{min}^{-1}$. Thermogravimetric analyses (TGA; Q500, TA Instruments, Inc., New Castle, DE, USA) of the compact material were performed starting at room temperature and heated to 800 °C under nitrogen or synthetic air (50 ml/min) with a heating rate of $10 \text{ K}\cdot\text{min}^{-1}$.

Cone calorimetric measurements (Fire Testing Technology Ltd, East Grinstead, England) of fiber-reinforced specimens were carried out in order to determine reaction-to-fire characteristics such as heat release, mass loss, formation of smoke etc. [35] according to ISO 5660 [36] in non-scrubbed mode. Specimens ($100 \times 100 \text{ mm}^2$) were wrapped in aluminum foil at the backside, supported on mineral wool, inserted in a frame sample holder and irradiated at a heat flux of $60 \text{ kW}\cdot\text{m}^{-2}$ for reinforced samples and at a heat flux of $35 \text{ kW}\cdot\text{m}^{-2}$ for neat resin samples. $60 \text{ kW}\cdot\text{m}^{-2}$ correspond more to fully developed fires and are used to observe the fiber degradation while $35 \text{ kW}\cdot\text{m}^{-2}$ correspond to

developing fires [37]. Test duration (5 min, 10 min, 20 min, 25 min) was varied for further investigations. Temperature rises were recorded by thermocouples (type K) attached to the front side of the specimens by a high-temperature resistant tape. The thermocouples were located close to the center of each panel.

Table 1. Prepared samples based on RTM6 resin.

Flame Retardant in RTM6-Matrix	Reinforcement	Thickness/mm
-	-	4
10% TAHHT-DOPO	-	4
10% TAHHT-DDPO	-	4
10% TAHHT-DOPO-DDPO	-	4
-	CF	2
10% BA-DOPO	CF	2
10% TAHHT-DOPO	CF	2
10% TAHHT-DDPO	CF	2
10% TAHHT-DOPO-DDPO	CF	2
35% Actilox B30	-	4
30% Actilox B30 + 5% TAHHT-DDPO	-	4
30% Actilox B30 + 5% TAHHT-DOPO	-	4
35% Disperal 40	-	4
30% Disperal 40 + 5% TAHHT-DDPO	-	4
30% Disperal 40 + 5% TAHHT-DOPO	-	4

CF: carbon fiber.

A scanning electron microscope (SEM; SM-300, TOPCON Corp., Tokyo, Japan) was used for the determination of fiber diameters. For each given value, the diameters of at least 30 fibers are averaged. Energy-dispersive X-ray spectroscopy (EDX) analyses were done on an EVO HD 25 (Carl Zeiss Microscopy GmbH, Jena, Germany) scanning electron microscope.

Interlaminar shear strength (ILSS) tests were performed for 2 mm thick specimens in accordance to EN 2563 by a three-point flexural test with a universal mechanical testing machine (Z020, ZwickRoell GmbH & Co. KG, Ulm, Germany) [38].

3. Results and Discussion

3.1. Characterization of Phosphorus-Containing Polyacrylamides

The thermal stability of the newly synthesized polymeric flame retardants was determined by TG analysis. The temperature at maximum mass loss rate (T_{max}), the initial degradation temperatures ($T_{1\%}$, $T_{5\%}$) at which 1% or 5% mass loss is reached and the residue at 800 °C are summarized in Table 2.

Table 2. T_{max} , $T_{1\%}$, $T_{5\%}$ and residue of phosphorus containing polyacrylamides obtained by thermogravimetric (TG) measurements in air or under nitrogen atmosphere with a heating rate of 10 K·min⁻¹.

Sample	$T_{max}/^{\circ}\text{C}$	$T_{1\%}/^{\circ}\text{C}$	$T_{5\%}/^{\circ}\text{C}$	Residue/%
BA-DOPO, N ₂	323	220	281	15 (800 °C)
TAHHT-DOPO	337	231	307	10 (800 °C)
TAHHT-DDPO	287	181	255	19 (800 °C)
TAHHT-DOPO-DDPO	315	220	268	9 (800 °C)
BA-DOPO, air	I 335 II 549 III 717	178	290	25 (453 °C) 7 (800 °C)
TAHHT-DOPO	I 237 II 300	237	300	25 (544 °C) 6 (800 °C)
TAHHT-DDPO	I 280 II 526 III 699	209	250	33 (419 °C) 14 (800 °C)
TAHHT-DOPO-DDPO	I 317 II 472	213	268	22 (420 °C) 8 (800 °C)

Figure 2 shows that DOPO-containing flame retardants like BA-DOPO and TAHHT-DOPO decompose at higher temperatures ($T_{5\%,N_2} = 281$ °C/307 °C) than DDPO-containing flame retardants

like TAHHT-DDPO ($T_{5\%,N_2} = 255\text{ }^\circ\text{C}$) under nitrogen atmosphere. The thermal stability of TAHHT-DOPO-DDPO is a combination of the thermal stabilities of TAHHT-DOPO and TAHHT-DDPO ($T_{5\%,N_2} = 268\text{ }^\circ\text{C}$), as expected. The residue is highest for TAHHT-DDPO (19%). The results of measurements in synthetic air are shown in Figure 3. After similar initial degradation temperatures for measurements under nitrogen atmosphere and the char formation in the first step, this residue, that is highest for TAHHT-DDPO (33% at $419\text{ }^\circ\text{C}$), is decomposed slowly.

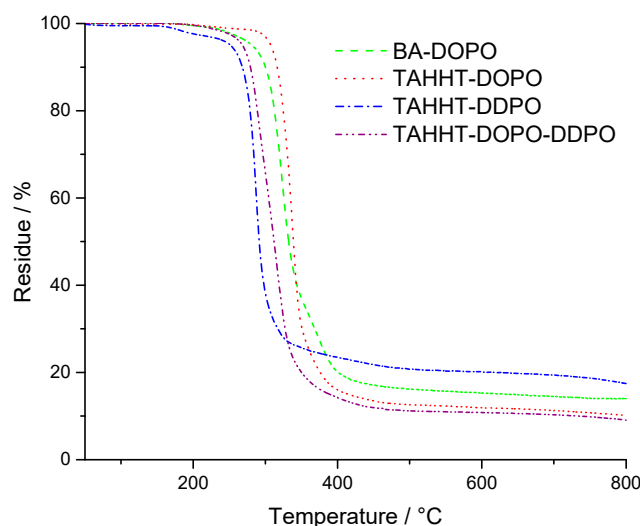


Figure 2. TG-curves of phosphorus containing polyacrylamides measured under N_2 -atmosphere.

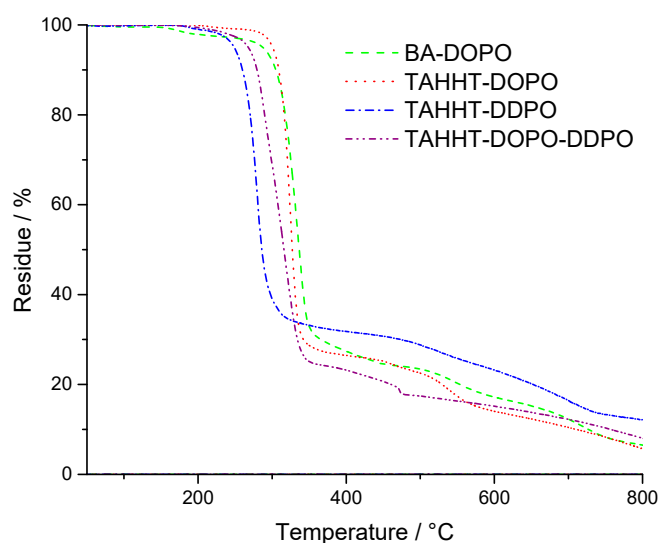


Figure 3. TG-curves of phosphorus containing polyacrylamides measured in air.

3.2. Neat Resin Samples and Carbon Fiber-Reinforced Composites

3.2.1. Material Characterization

Glass transition temperatures were determined by dynamic mechanical analysis (DMA) as the maximum of the dissipation factor $\tan(\delta)$: $T_g(\text{Max}(\tan(\delta)))$. The results are shown in Table 3. The incorporation of 10% phosphorus containing polyacrylamides leads to a maximum decrease of $13\text{ }^\circ\text{C}$, meaning a minor change of the glass transition temperature according to literature [1,24]. This change is caused by the low plasticizer effect of the oligomeric structures.

Table 3. Glass transition temperatures and moisture uptake of RTM6 samples.

Sample	$T_g(\text{Max}(\tan(\delta)))$ ¹ / $^{\circ}\text{C}$	Moisture uptake/%	$T_{g,\text{wet}}(\text{Max}(\tan(\delta)))$ ¹ / $^{\circ}\text{C}$
RTM6	215	1.02	218
+ 10% BA-DOPO	208	1.02	205
+ 10% TAHHT-DOPO	205	1.02	202
+ 10% TAHHT-DDPO	202	1.03	198
+ 10% TAHHT-DOPO-DDPO	204	1.02	197

¹ Error in measurement ± 3 $^{\circ}\text{C}$.

Moisture uptake was determined by storing samples in water at 70 $^{\circ}\text{C}$ for 14 days. The increase in mass compared to the initial mass is 1.02% for the pure RTM6 and all other samples except for TAHHT-DOPO with 1.03%. According to this, the flame retardants have almost no influence on the moisture uptake. Glass transition temperatures of wetted samples ($T_{g,\text{wet}}$) are similar to the temperatures of the original samples, because drying occurs before the glass temperature is reached. Slight decreases of the glass transition temperatures are observed since the hydrophilic phosphorous species prevent a complete drying in the given timespan. However, these changes are insignificant.

Table 4 presents interlaminar shear strength (ILSS) of the investigated CFRP samples. Values are additionally normalized to the CFRP without flame retardants. The incorporation of 10% polyacrylamides leads to no significant change of ILSS, which is within the measurement tolerance of the testing method ($\pm 10\%$). Therefore the application of the investigated flame retardants in epoxy based composites is possible with respect to mechanical performance.

Table 4. Interlaminar shear strength (ILSS) of selected carbon fiber-reinforced thermoset polymers (CFRP) samples additionally normalized to RTM6 + CF.

Sample	ILS ($\text{N}\cdot\text{mm}^{-2}$)	Relative ILSS (%)
RTM6 + CF	67.8 ± 3.2	100 ± 5
+ 10% BA-DOPO	65.4 ± 2.0	97 ± 3
+ 10% TAHHT-DOPO	67.4 ± 1.8	99 ± 3
+ 10% TAHHT-DDPO	71.0 ± 2.3	105 ± 4

3.2.2. Thermal Properties

The thermal properties of the flame retardants and RTM6 formulations thereof were investigated by TGA under nitrogen atmosphere and in air. Figure 4 shows one step decomposition processes for RTM6 and flame retarded formulations under nitrogen atmosphere and Figure 5 shows two step decomposition processes in air. The temperature at maximum mass loss rate (T_{max}), the initial degradation temperatures ($T_{1\%}$, $T_{5\%}$) at which 1% or 5% mass loss is reached and the residue at 800 $^{\circ}\text{C}$ are summarized in Table 5.

Under nitrogen atmosphere, the initial degradation temperatures $T_{1\%}$ and $T_{5\%}$ are lowered for every flame retardant, which indicates a flame-retarding action before the decomposition of the overall matrix. The residues are higher for flame retarded samples indicating the formation of char. It is highest for TAHHT-DDPO with 19%. The high residue shows a strong charring effect of TAHHT-DDPO in RTM6 resulting from the formation of polyphosphoric acid and the catalysis of the carbonification of the cured resin [39,40]. This charring layer is efficient to form a heat-barrier during combustion. RTM6 samples with other polyacrylamides added show higher residues than neat RTM6 as well.

The simplified decomposition model by Rose and co-workers [41,42] assumes three steps for the decomposition of epoxy resins in air. An undistinctive first step is caused by dehydration leading to the formation of a moisture-free resin system. In a temperature range of 300 $^{\circ}\text{C}$ to 450 $^{\circ}\text{C}$, the decomposition into stable char and different volatile species takes place. The third reaction taking place at temperatures above 450 $^{\circ}\text{C}$ is responsible for further degradation of the stable char. For RTM6 and DOPO-containing polyacrylamides, more volatiles are set free in the first decomposition step,

leading to fewer residues before the second decomposition step occurs, suggesting gas-phase activity for these flame retardants.

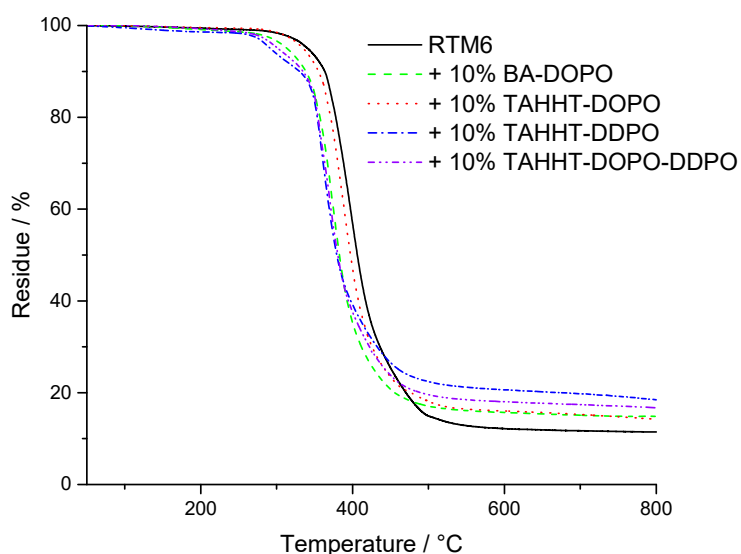


Figure 4. TG-curves of RTM6 and flame-retarded samples measured under N₂-atmosphere.

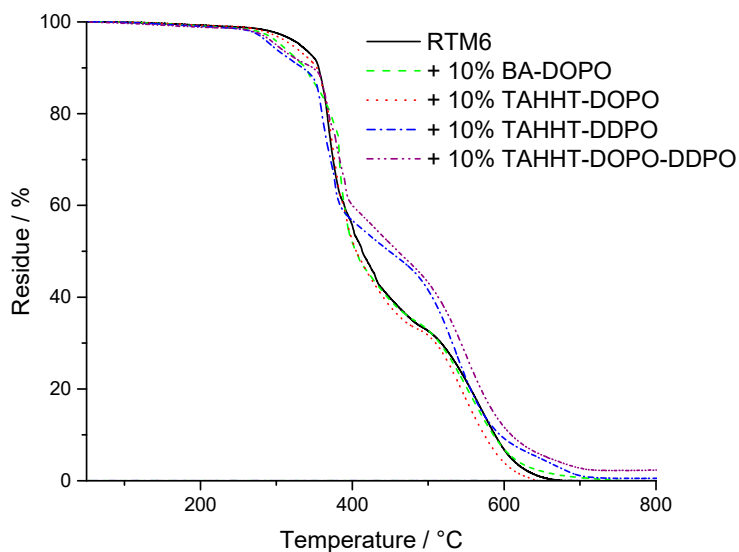


Figure 5. TG-curves of RTM6 and flame-retarded samples measured under air.

Table 5. T_{max}, T_{1%}, T_{5%} and residue of formulations of RTM6 and phosphorus containing flame retardants obtained by TG measurements under air or nitrogen atmosphere with a heating rate of 10 K·min⁻¹.

Sample	T _{max} /°C	T _{1%} /°C	T _{5%} /°C	Residue/%
RTM6, N ₂	379	265	341	10 (800 °C)
+ 10% BA-DOPO	373	211	314	15 (800 °C)
+ 10% TAHHT-DOPO	389	284	335	14 (800 °C)
+ 10% TAHHT-DDPO	362	170	293	19 (800 °C)
+ 10% TAHHT-DOPO-DDPO	371	216	301	17 (800 °C)
RTM6, air	I 369 II 572	229	331	33 (492 °C) 0 (800 °C)
+ 10% BA-DOPO	I 384 II 555	198	305	34 (488 °C) 0 (800 °C)
+ 10% TAHHT-DOPO	I 373 II 546	212	318	34 (479 °C) 0 (800 °C)
+ 10% TAHHT-DDPO	I 360 II 376 III 537	198	293	52 (433 °C) 1 (800 °C)
+ 10% TAHHT-DOPO-DDPO	I 301 II 368 III 550	190	301	51 (454 °C) 3 (800 °C)

3.2.3. Flame-Retardant Performance

Fire tests of the neat resin (4 mm samples) under forced conditions were done at a heat flux of $35 \text{ kW}\cdot\text{m}^{-2}$ in a cone calorimeter. This heat flux is suitable for the investigation of the burning behavior. Composite materials (2 mm samples) were investigated at a heat flux of $60 \text{ kW}\cdot\text{m}^{-2}$ respectively to quantifiably observe the fiber degradation within 20 min. The HRR (heat release rate) curves vs. time of neat resins are presented in Figure 6 and the curves of the composites in Figure 7. Values of important parameters including time to ignition (tti), peak of heat release rate (pHRR), total heat release (THR), maximum average rate of heat emission (MARHE) and the total smoke release (TSR) values are summarized in Table 6. For the 2 mm reinforced samples the sum parameters were determined after 300 s of testing and for the 4 mm neat resin samples after 500 s. Hand lay-up leads to different fiber volume ratios, so the combustible material amount differs for the different reinforced samples, which is considered by the value X as the ratio of the combustible material mass (equal to the mass of the matrix) to the whole sample mass. In addition UL94-test classifications of 4 mm thick samples are specified in Table 6.

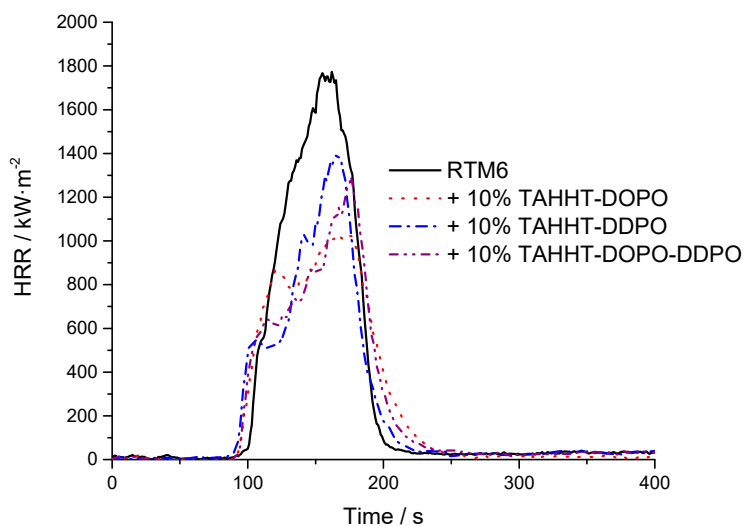


Figure 6. Heat release rate (HRR) of non-reinforced samples at $35 \text{ kW}\cdot\text{m}^{-2}$.

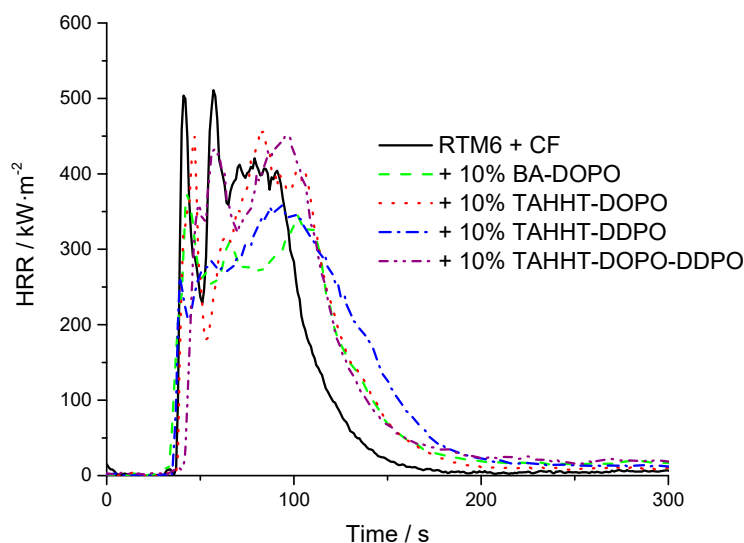


Figure 7. HRR of reinforced samples at $60 \text{ kW}\cdot\text{m}^{-2}$.

Table 6. Results of cone calorimetry (neat resin: sample thickness 4 mm, composites: sample thickness 2 mm) and UL94 (sample thickness 4 mm) for depicted samples.

Sample	t _{ti} /s	pHRR/kW·m ⁻²	THR·X ⁻¹ /MJ·m ⁻²	MARHE/kW·m ⁻²	TSR·X ⁻¹ /m ² ·m ⁻²	THR·ML ⁻¹¹ /kW·m ⁻² ·g ⁻¹	Residue/%	X	UL94-V *
RTM6	94 ± 1	1715 ± 58	104 ± 1	550 ± 6	5601 ± 31	2.25	4 ± 2	1	NR
+ 10% BA-DOPO	-	-	-	-	-	-	-	1	V1
+ 10% TAHHT-DOPO	98 ± 12	1092 ± 54	89 ± 2	401 ± 22	6458 ± 51	1.85	2 ± 0	1	V0
+ 10% TAHHT-DDPO	81 ± 2	1419 ± 8	85 ± 2	421 ± 3	3853 ± 17	2.19	3 ± 0	1	V0
+ 10% TAHHT-DOPO-DDPO	85 ± 1	1278 ± 30	85 ± 3	416 ± 8	5160 ± 123	1.97	2 ± 0	1	V0
RTM6 + CF	31 ± 2	492 ± 19	72 ± 1	242 ± 5	3763 ± 165	2.51	59 ± 1	0.43	V1
+ 10% BA-DOPO	32 ± 5	384 ± 53	63 ± 3	203 ± 16	5815 ± 600	2.05	56 ± 1	0.49	V0
+ 10% TAHHT-DOPO	34 ± 1	476 ± 75	70 ± 3	234 ± 115	5070 ± 283	2.17	54 ± 1	0.52	V0
+ 10% TAHHT-DDPO	29 ± 4	388 ± 52	67 ± 4	218 ± 22	4277 ± 369	2.37	59 ± 1	0.50	V0
+ 10% TAHHT-DOPO-DDPO	37 ± 3	456 ± 58	69 ± 2	228 ± 13	5269 ± 136	2.21	55 ± 1	0.52	V0

X: ratio of the combustible material mass to the whole sample mass. * NR: not rated.

The burning behavior of neat RTM6 is characterized by a sharp peak in HRR, which is characteristic for a rapid and continuous combustion. For flame retarded samples the development of the HRR during the measurement shows a lower heat release shortly after burning, resulting in a peak at a comparable time to the non-flame retarded sample. The addition of flame retardants to RTM6 leads to decreasing pHRR-, THR- and MARHE-values. The reduction of pHRR is the highest for the sample flame retarded with TAHHT-DOPO by 36%. Literature [9] showed a comparable effect of other DOPO and DDPO-containing flame retardants in neat RTM6 samples. In particular the addition of TAHHT-DDPO leads to a decrease of the HRR just after ignition which is essential for the further burning process as the decrease of HRR indicates the formation of char [37]. The addition of TAHHT-DOPO delays the tti whereas DDPO-containing polyacrylamides decrease the tti. This observation is characteristic, because the gas phase activity of DOPO inhibits the ignition whereas a char is not formed before combustion.

UL94 measurements show that an addition of 10 wt% of flame retardants results in V0 classifications for all samples except for BA-DOPO. The fiber reinforcement acts as inert filler. Therefore, the RTM6-composite reaches V1 classification even without an additional flame retardant and V0 classification for flame-retarded samples. The fiber-reinforcement leads to significant differences in the HRR-curves in comparison to non-reinforced material. Delamination processes are represented in the curves by sharp peaks shortly after ignition. Single plies are detached from others and they burn fierce and fast due to gas between the fiber plies acting as a heat barrier. The reinforcement significantly reduces pHRR, THR, MARHE and TSR. The relative changes caused by the incorporation of flame retardants are comparable to the non-reinforced samples, but the high heat flux of $60 \text{ kW}\cdot\text{m}^{-2}$ required for fiber degradation leads to significant standard deviations, so that the detailed comparison of the different flame retardants is not possible.

The THR/ML (ML: mass loss) value gives reliable information on the flame retardant mechanism [37] as it stands for the total heat evolved per mass that is released in form of volatiles. The smaller this value is in comparison to the non-flame retarded sample (non-reinforced: $2.25 \text{ kW}\cdot\text{m}^{-2}\cdot\text{g}^{-1}$ /reinforced: $2.51 \text{ kW}\cdot\text{m}^{-2}\cdot\text{g}^{-1}$), the more gas phase activity occurs during combustion. According to the value of THR/ML, TAHHT-DDPO acts mainly in the condensed phase (non-reinforced: $2.19 \text{ kW}\cdot\text{m}^{-2}\cdot\text{g}^{-1}$ /reinforced: $2.37 \text{ kW}\cdot\text{m}^{-2}\cdot\text{g}^{-1}$) which is also shown by the low $\text{TSR}\cdot\text{X}^{-1}$ ($3853 \text{ m}^2\cdot\text{m}^{-2}$) of the non-reinforced sample. DOPO containing polyacrylamides show a distinctive gas phase activity.

The overall amount of formed smoke ($\text{TSR}\cdot\text{X}^{-1}$) is higher for flame retarded composite samples than for the non-flame retarded samples.

Figure 8 shows SEM images of the residues obtained after cone calorimetry at $35 \text{ kW}\cdot\text{m}^{-2}$ for 10 min. While RTM6 alone forms a highly instable residue that contains small holes (diameter about 50–100 μm), the addition of phosphorus containing flame retardants leads to residues that are more stable and covered with less holes. In particular, the addition of TAHHT-DDPO to RTM6 shows a continuous layer.

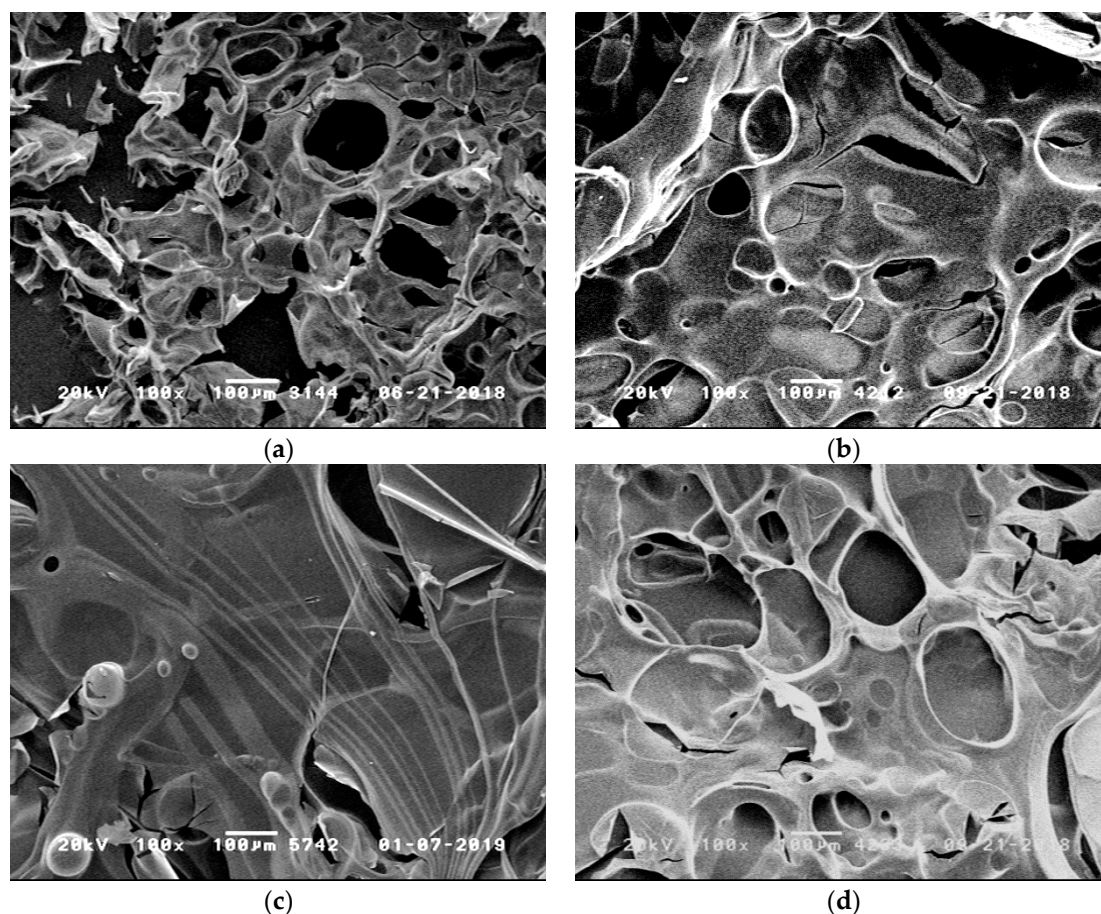


Figure 8. Scanning electron microscope (SEM) images of the residues obtained after cone calorimetry at $35 \text{ kW}\cdot\text{m}^{-2}$ for 10 min: (a) RTM6; (b) RTM6 + 10% TAHHT-DOPO; (c) RTM6 + 10% TAHHT-DDPO; (d) RTM6 + 10% TAHHT-DOPO-DDPO.

3.2.4. Fiber Protection

SEM was used to determine mean diameters and smallest fiber diameters of carbon fibers for different samples shown in Table 7. The determined initial diameter of G0939 carbon fibers is $(7.3 \pm 0.3) \mu\text{m}$. For composites not containing any flame retardant a mean fiber diameter of $(3.3 \pm 0.7) \mu\text{m}$ and a mentionable amount of respirable fiber fragments are observed after irradiation at $60 \text{ kW}\cdot\text{m}^{-2}$ (20 min). For each investigated flame retardant, no respirable fiber fragments were observed under the same conditions. The incorporation of TAHHT-DDPO showed the best fiber protection with a mean fiber diameter of $(6.3 \pm 0.4) \mu\text{m}$ after irradiation at $60 \text{ kW}\cdot\text{m}^{-2}$ (20 min). Flame retardants that contain only DOPO as phosphorus source, show slightly smaller mean fiber diameters (BA-DOPO: $(5.2 \pm 0.3) \mu\text{m}$, TAHHT-DOPO: $(5.3 \pm 0.2) \mu\text{m}$). The different substituted polyacrylamide TAHHT-DOPO-DDPO shows a mean fiber diameter of $(5.9 \pm 0.3) \mu\text{m}$ after irradiation that is in between the mean diameters of the flame retardants with only one phosphorus source, as expected.

Figure 9 shows the mean fiber diameter depending on irradiation time at $60 \text{ kW}\cdot\text{m}^{-2}$ for different resin formulations. Carbon fibers in RTM6 without addition of flame retardants show a steady decrease in diameter. After 5 min a mean diameter of $(6.6 \pm 0.4) \mu\text{m}$ is reached, after 20 min $(3.3 \pm 0.7) \mu\text{m}$. Within the observed irradiation time of 20 min, the fiber degradation is retarded sufficiently by addition of any phosphorus containing polyacrylamide. After 300 s no significant degradation of the fiber diameter occurs. The results for BA-DOPO and TAHHT-DOPO show similar curve progressions. TAHHT-DDPO is the most effective flame retardant for fiber protection. The curve for TAHHT-DOPO-DDPO containing samples is in between, as expected. An additional composite

containing 10% TAHHT-DOPO-DDPO that was irradiated for 1500 s still exhibits a mean diameter of $(5.4 \pm 0.3) \mu\text{m}$. Figure 10 shows SEM images of carbon fibers after irradiation at $60 \text{ kW}\cdot\text{m}^{-2}$. While the composite which does not contain any flame retardants (Figure 10a) tends to form holes at the fiber surface within 1200 s, the sample with 10% TAHHT-DOPO-DDPO shows no defects after 1500 s (Figure 10b).

Table 7. Mean diameter, standard deviation and smallest measured diameter of at least 30 carbon fibers in composite materials with partially flame retarded RTM6 after irradiation at $60 \text{ kW}\cdot\text{m}^{-2}$ for 20 min determined by SEM.

Sample	Mean Diameter (μm)	Smallest Diameter (μm)
RTM6 + CF	3.3 ± 0.7	2.1
+ 10% BA-DOPO	5.2 ± 0.3	4.7
+ 10% TAHHT-DOPO	5.3 ± 0.2	4.9
+ 10% TAHHT-DDPO	6.3 ± 0.4	5.3
+ 10% TAHHT-DOPO-DDPO	5.9 ± 0.3	5.3

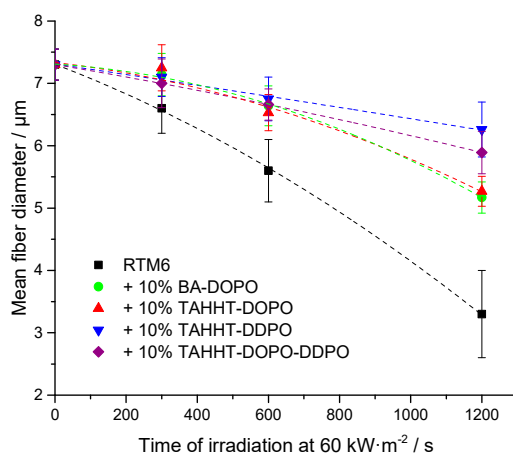


Figure 9. Mean fiber diameter in dependence on irradiation time at $60 \text{ kW}\cdot\text{m}^{-2}$ and flame retarded matrix composition.

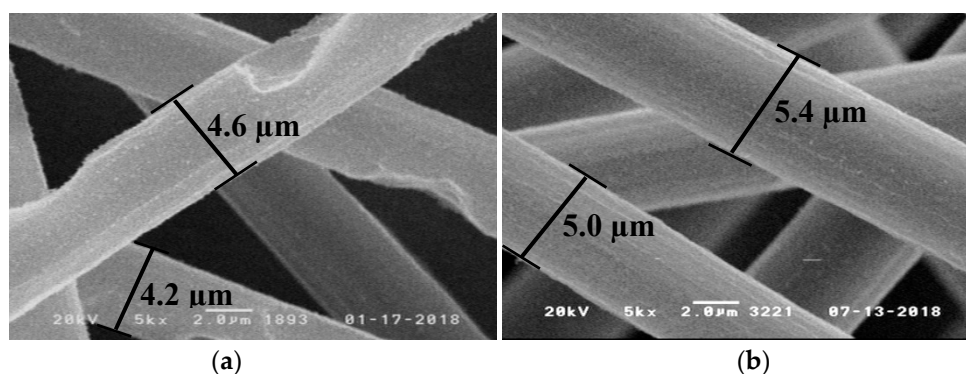


Figure 10. SEM images of carbon fibers after irradiation at $60 \text{ kW}\cdot\text{m}^{-2}$: a: RTM6 + CF, 1200 s; b: RTM6 + 10% TAHHT-DOPO-DDPO, 1500 s.

In order to determine the mechanism of fiber protection, the temperature on the irradiated surface during combustion was measured by a thermocouple attached to the sample. The results are shown in Figure 11. Temperatures above $600 \text{ }^\circ\text{C}$ necessary for fiber degradation [15] are reached during the combustion of the matrix resin. There are no distinct differences in the shape of these curves suggesting

that there is no influence of the surface temperature on the resulting mean fiber diameter, but the added flame retardants are responsible for fiber protection.

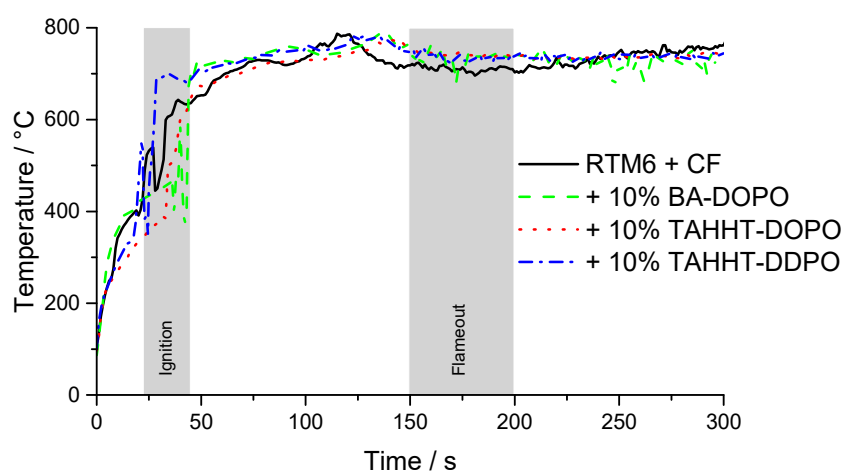


Figure 11. Temperature at the sample surface during irradiation ($60 \text{ kW}\cdot\text{m}^{-2}$) measured by a thermocouple attached to the surface.

The results of EDX measurements are summarized in Table 8. After 1200 s at $60 \text{ kW}\cdot\text{m}^{-2}$, the surface of carbon fibers in the non-flame retarded composite sample consists of 94.3% carbon, 4.2% nitrogen and 1.4% oxygen. Interestingly, DDPO-containing samples show higher P- and O-contents on the fiber surface after irradiation. The incorporation of TAHHT-DOPO leads to 0.7% P and 2.8% O on the fiber surface after irradiation. Whereas TAHHT-DDPO containing samples showed 2.4% P and 8.8% O and TAHHT-DOPO-DDPO containing samples showed 1.4% P and 6.8% O on the fiber surface after irradiation. This corresponds to the predicted activity in the condensed phase for DDPO by the formation of polyphosphoric acid. However, with prolonged irradiation polyphosphoric acid is degraded and fiber protection decreases. During the irradiation under the cone heater a loose matrix residue is obtained on top of the sample and between the laminate plies that is decreased constantly during the run.

Table 8. Concentrations of elements at the fiber surface after irradiation.

Sample	C on surface/%	N on surface/%	O on surface/%	P on surface/%
RTM6 + CF 1200 s at $60 \text{ kW}\cdot\text{m}^{-2}$	94.3	4.2	1.4	not detected
+ 10% TAHHT-DOPO 1200 s at $60 \text{ kW}\cdot\text{m}^{-2}$	91.9	4.6	2.8	0.7
+ 10% TAHHT-DDPO 1200 s at $60 \text{ kW}\cdot\text{m}^{-2}$	84.0	4.3	8.8	2.4
+ 10% TAHHT-DOPO-DDPO 1200 s at $60 \text{ kW}\cdot\text{m}^{-2}$	86.3	4.9	6.8	1.4

3.3. Synergistic Mixtures with Boehmite

3.3.1. Thermal Properties

The thermal properties of RTM6 formulations with boehmite and the phosphorus-containing flame retardants TAHHT-DDPO and TAHHT-DOPO were determined by TG measurements. Two types of boehmite were tested: synthetic boehmite Actilox[®] B30 (Actilox) and Disperal[®] 40 (Disperal). Actilox[®] B30 is a high purity boehmite (99%) with a particle size D_{50} of 1.8 μm and specific surface area (BET) of $3 \text{ m}^2\cdot\text{g}^{-1}$. Disperal[®] 40 is an acid dispersable boehmite with lower purity (94%) and bigger particles (35 μm) with higher BET-surface ($100 \text{ m}^2\cdot\text{g}^{-1}$) [43,44].

The results for the temperature at maximum mass loss rate (T_{max}), the initial degradation temperatures ($T_{1\%}$, $T_{5\%}$) at which 1% or 5% mass loss is reached and the residue at 800 °C are summarized in Table 9. Measurements under nitrogen atmosphere showed similar results for samples containing Actilox (Figure 12) and Disperal (Figure 13) in terms of temperatures at 5% mass lost and residue. In combination with TAHHT-DOPO the temperatures with 1% and 5% mass lost are not affected significantly for Actilox-containing samples. The temperature with 1% mass lost is increased by 20 °C to 305 °C for Disperal-containing samples. The residue at 800 °C is increased by 5% with Actilox and 2% with Disperal. The temperature at 1% mass lost is decreased by more than 20 °C for both boehmite types with TAHHT-DDPO. On the other hand, the temperature at 5% mass lost is just decreased slightly by TAHHT-DDPO with both types of boehmite. With this phosphorus containing compound, the residue is significantly higher, leading to 46% residue at 800 °C for Disperal + TAHHT-DDPO.

Table 9. T_{max} , $T_{1\%}$, $T_{5\%}$ and residue of boehmite and phosphorus containing polyacrylamides in RTM6 obtained by TG measurements under nitrogen atmosphere or synthetic air with a heating rate of 10 K·min⁻¹.

Sample	$T_{max}/^{\circ}\text{C}$	$T_{1\%}/^{\circ}\text{C}$	$T_{5\%}/^{\circ}\text{C}$	Residue/%
RTM6, N ₂	379	265	341	10 (800 °C)
+ 30% Actilox	376	301	343	29 (800 °C)
+ 30% Actilox + 5% TAHHT-DDPO	373	274	333	37 (800 °C)
+ 30% Actilox + 5% TAHHT-DOPO	379	304	342	34 (800 °C)
+ 30% Disperal	374	285	353	30 (800 °C)
+ 30% Disperal + 5% TAHHT-DDPO	380	277	349	46 (800 °C)
+ 30% Disperal + 5% TAHHT-DOPO	376	305	346	33 (800 °C)
RTM6, air	I 369 II 572	229	331	33 (492 °C) 0 (800 °C)
+ 30% Actilox	I 366 II 538	215	348	64 (458 °C) 23 (800 °C)
+ 30% Actilox + 5% TAHHT-DDPO	I 371 II 394 III 558	267	329	66 (453 °C) 24 (800 °C)
+ 30% Actilox + 5% TAHHT-DOPO	I 371 II 409 III 534	299	354	60 (456 °C) 27 (800 °C)
+ 30% Disperal	I 386 II 543	267	350	60 (439 °C) 25 (800 °C)
+ 30% Disperal + 5% TAHHT-DDPO	I 383 II 581	267	343	61 (474 °C) 26 (800 °C)
+ 30% Disperal 40 + 5% TAHHT-DOPO	I 376 II 404 III 530	295	353	61 (445 °C) 25 (800 °C)

* NR: not rated.

TG measurements under synthetic air show similar results to measurements under nitrogen atmosphere. There is no significant difference between samples containing Actilox or Disperal except for RTM 6 + 30% Actilox. Its temperature at 1% mass lost is 52 °C lower than for the equivalent Disperal-containing sample. The incorporation of any phosphorus containing polyacrylamide leads to higher temperatures at 1% mass lost and lower temperatures at 5% mass lost. The residues at 800 °C are higher as well, but lower than under nitrogen. The graphs show just one decomposing step under nitrogen, but two steps under synthetic air (Figures 14 and 15). The first step is correlated to char formation. The second step, which is more distinctive for Actilox-containing samples, is correlated to char decomposition and formation of more volatiles. The reaction of boehmite to aluminum oxide occurs at similar temperatures like the decomposition of char [41,42]. This step occurs for all formulations between 510 and 530 °C. The temperatures of highest mass lost rate for the first maximum are about 370 °C and not affected significantly by the different flame retardants as well as the second maximum between 530 and 540 °C. The formulations with TAHHT-DDPO have a

higher last T_{max} , leading to the highest T_{max} at 581 °C for Disperal + TAHHT-DDPO. For the samples containing synergists, there is another peak around 400 °C. These peaks do not differ for the different formulations except for Disperal + TAHHT-DDPO with a missing peak. This step overlaps with the step of char formation.

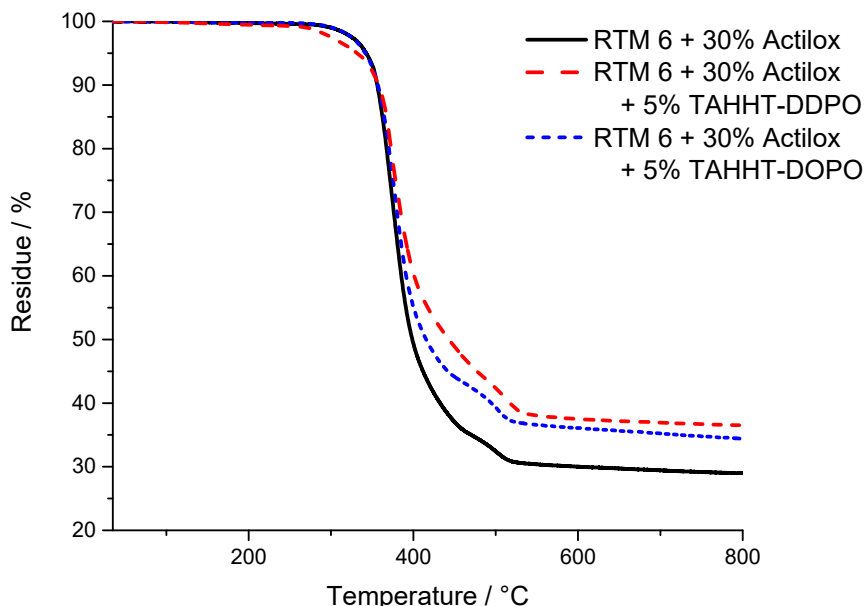


Figure 12. TG curves of Actilox-containing samples measured under N_2 -atmosphere.

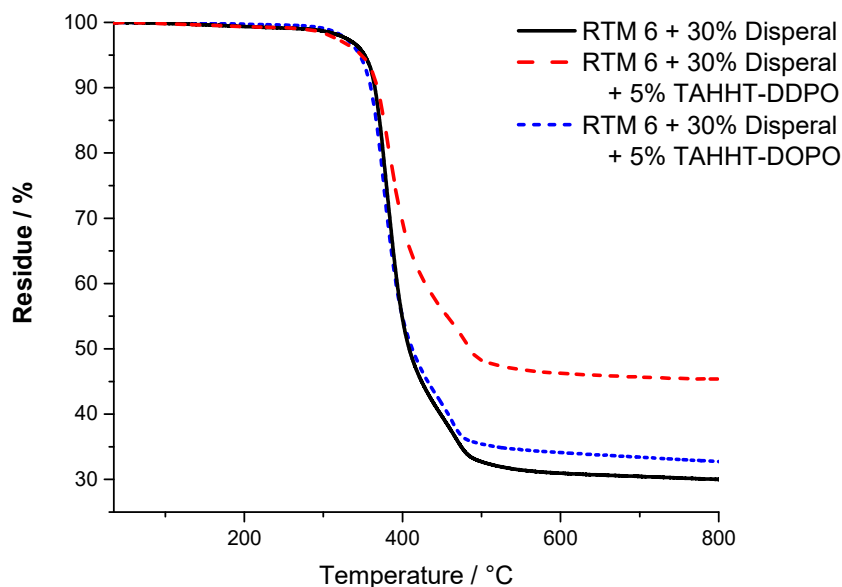


Figure 13. TG curves of Disperal-containing samples measured under N_2 -atmosphere.

For comparing purposes, the residue at the inflection point is examined. This point differs in residue and temperature between Actilox- and Disperal-containing specimens. On the one hand for Actilox-containing samples, the temperatures do not differ significantly. The residue is for TAHHT-DDPO slightly higher and for TAHHT-DOPO lower. On the other hand for Disperal-containing samples, the residue is constantly about 61%. But the temperature of the inflection point rises with synergists. Therefore the combination of TAHHT-DDPO and Disperal in RTM6 causes the highest temperature at inflection point with 474 °C.

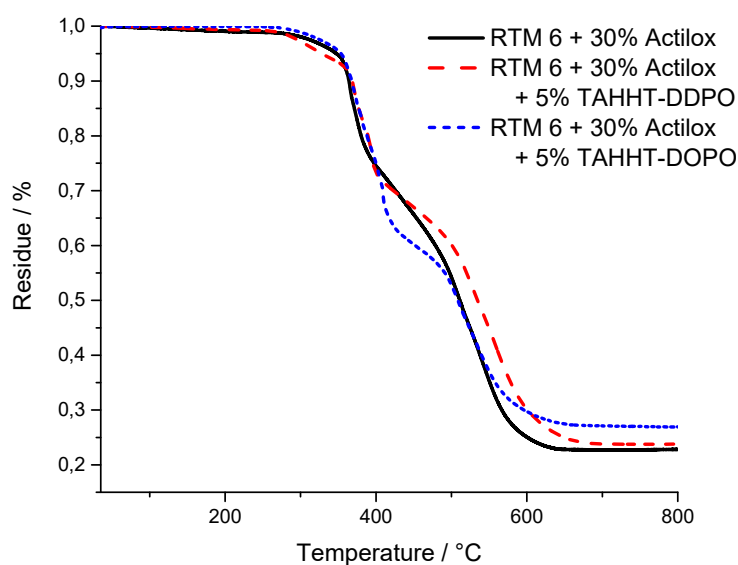


Figure 14. TG curves of Actilox-containing samples measured under air.

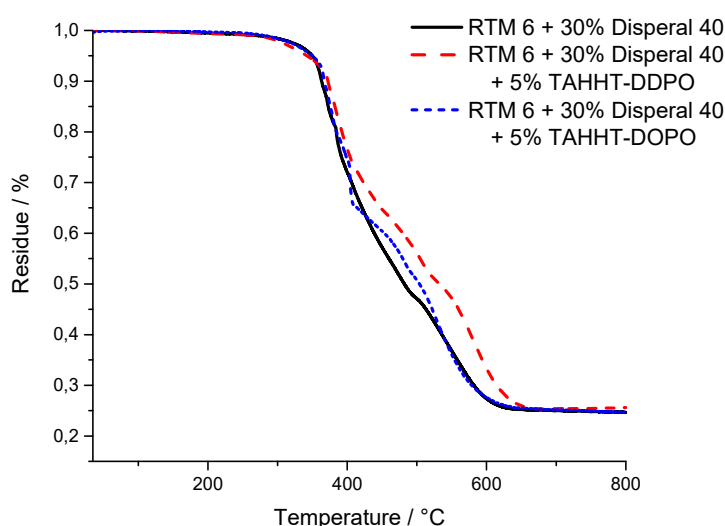


Figure 15. TG curves of Disperal-containing samples measured under air.

3.3.2. Flame-Retardant Performance

In order to determine the flame-retardant performance of different samples, UL94-tests and cone calorimetry measurements were performed. The results are summarized in Table 10. HRR curves are shown in Figures 16 and 17. In UL94 tests all specimens containing Disperal 40 reach no classification. Only a combination of Actilox B30 and TAHHT-DDPO in RTM6 achieves V0 rating. Results from cone calorimetry ($35 \text{ kW}\cdot\text{m}^{-2}$, 500 s) showed a delay of tti by 10 to 20 s for both boehmite types. The residue is increased by adding a synergist to Disperal-containing formulations. The residue of the specimen containing Actilox is not affected significantly by the incorporation of phosphorus-containing acrylamides. Other important parameters like pHRR, THR, MARHE and TSR are decreased. pHRR is decreased by boehmite additives, but also decreased by the addition of phosphorus containing polyacrylamides. It drops by 34% using Actilox B30 and by 22% with Disperal 40. Both synergists lower the pHRR with the formulation of TAHHT-DOPO and Actilox B30 in RTM6 having the lowest result. The pHRR is decreased by 46% to 919 kW m^2 . The additives affect not only the peak, but the whole curve (Figure 16). Whilst pure RTM6 shows a peak in HRR curve in the end of its burning, adding boehmite leads to broader, smaller peaks with maximum in the center.

Table 10. Results of cone calorimetry and UL94 (sample thickness 4 mm) for depicted samples containing boehmite.

Sample	t _{ti} /s	pHRR/kW·m ⁻²	THR/MJ·m ⁻²	MARHE/kW·m ⁻²	TSR/m ² ·m ⁻²	THR·ML ⁻¹ /kW·m ⁻² ·g ⁻¹	Residue/%	UL94-V *
RTM 6	94 ± 2	1715 ± 58	113 ± 2	550 ± 6	6305 ± 394	2.39	1.9 ± 1.4	NR
+ 35% Actilox B30	109 ± 12	1142 ± 14	107 ± 3	420 ± 13	5079 ± 94	2.38	5.7 ± 1.0	NR
+ 30% Actilox B30 + 5% TAHHT-DDPO	96 ± 5	1017 ± 60	99 ± 2	410 ± 1	4868 ± 118	2.24	33.6 ± 0.5	V0
+ 30% Actilox B30 + 5% TAHHT-DOPO	110 ± 4	919 ± 20	91 ± 3	359 ± 11	5309 ± 148	1.99	32.5 ± 0.7	NR
+ 35% Disperal 40	95 ± 7	1330 ± 22	102 ± 3	454 ± 22	4239 ± 249	2.11	25.8 ± 6.4	NR
+ 30 % Disperal 40 + 5% TAHHT-DDPO	108 ± 2	1289 ± 31	96 ± 3	423 ± 5	4511 ± 204	2.22	32.0 ± 0.7	NR
+ 30% Disperal 40 + 5% TAHHT-DOPO	117 ± 4	1065 ± 5	89 ± 4	372 ± 20	5261 ± 16	1.94	32.6 ± 1.1	NR

* NR: not rated.

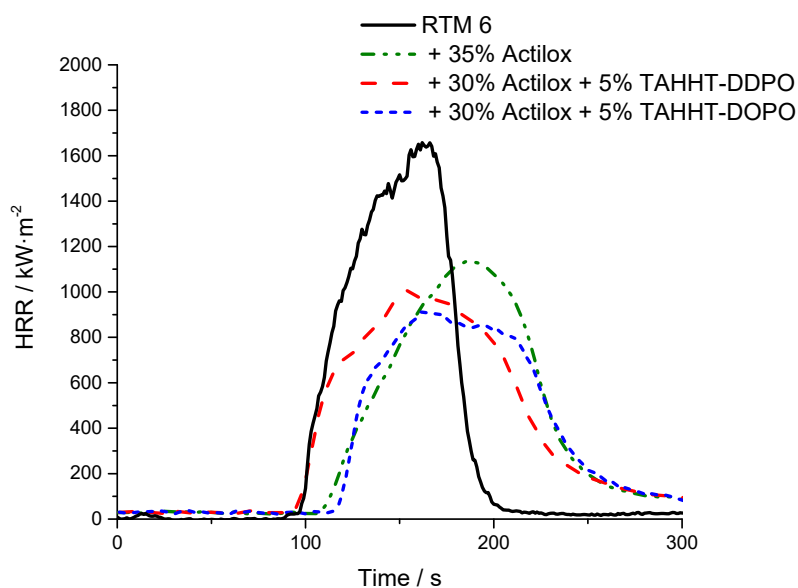


Figure 16. HRR of different specimen with and without Actilox B30 at $35 \text{ kW}\cdot\text{m}^{-2}$.

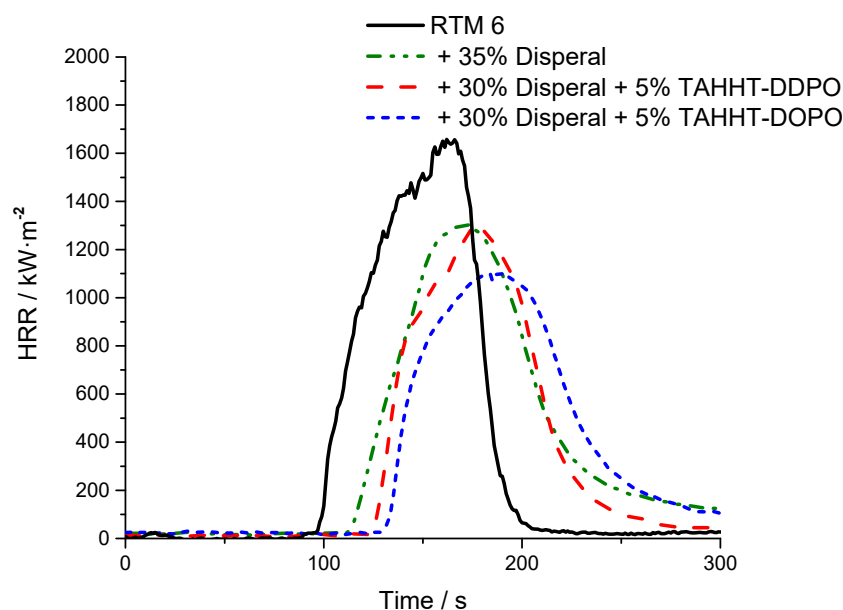


Figure 17. HRR of different specimen with and without Disperal 40 at $35 \text{ kW}\cdot\text{m}^{-2}$.

The THR/ML value gives reliable information on the flame-retardant mechanism [37] as it stands for the total heat evolved per mass that is released in form of volatiles. A decrease by 18% is observed using TAHHT-DOPO and boehmite in comparison to pure RTM 6. This indicates more gas-phase activity which can be conferred to an increase of TSR. The addition of TAHHT-DOPO leads to a small increase of TSR by 5% for Actilox B30, but it increases by 24% for Disperal 40. THR/ML and TSR do not distinguish significantly between the boehmite types in combination with each synergist. MARHE shows the same tendency. It is decreased by boehmite as well as by the synergists. It is affected most by the incorporation of TAHHT-DOPO leading to a decrease by 35% with Actilox B30 conferred to pure RTM 6.

Figure 18 shows SEM images of the residues obtained after cone calorimetry at $35 \text{ kW}\cdot\text{m}^{-2}$ for 500 s. The addition of Actilox B30 to RTM6 leads to a non-continuous char surface with fractures indicating a fragile surface. Holes remain suggesting the possibility of oxygen and heat exchange. Voluminous structures were obtained with TAHHT-DOPO and Actilox B30 in RTM6. Specimens

containing TAHHT-DDPO show a rough surface with a network-like structure underneath. Dispersal 40 leads to a small layer of rough surface without holes. In some spots, the surface is broken and shows little holes underneath like the samples with Actilox B30. This surface is nearly completely decomposed for TAHHT-DOPO indicating a high gas-phase activity of this flame retardant. Voluminous structures are not observed with Dispersal 40.

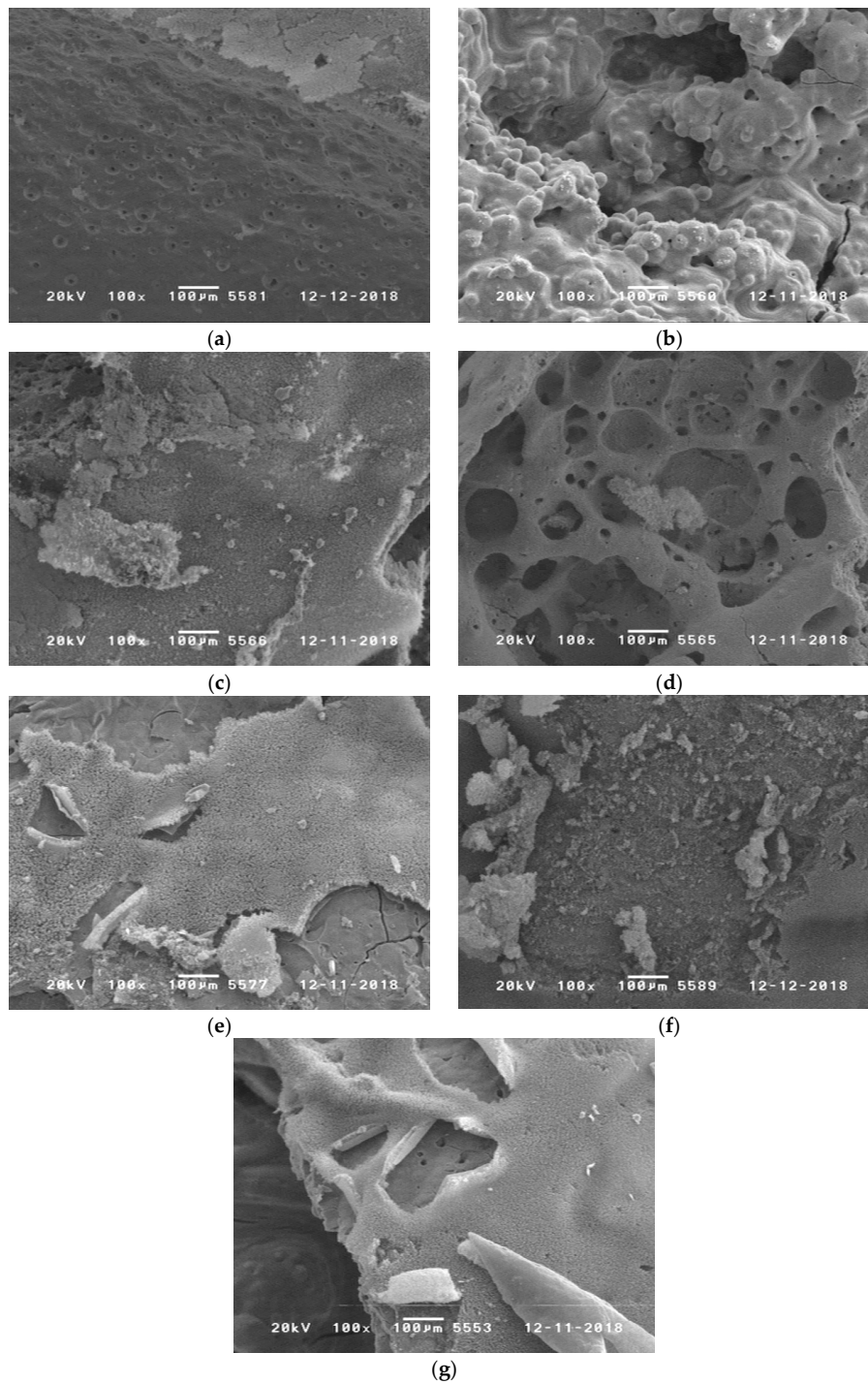


Figure 18. SEM images of the residues obtained after cone calorimetry for RTM6 samples at $35 \text{ kW}\cdot\text{m}^{-2}$ for 500 s with: (a) 35% Actilox; (b) 30% Actilox + 5 % TAHHT-DOPO; (c) 30% Actilox + 5% TAHHT-DDPO surface; (d) 30% Actilox + 5% TAHHT-DDPO inside a hole; (e) 35% Dispersal; (f) 30% Dispersal + 5% TAHHT-DOPO; (g) 30% Dispersal + 5% TAHHT-DDPO.

The pictures show that during combustion a brittle char is developed. Only for V0 rating, a firm char layer is needed in order to inhibit oxygen and gas exchange [31]. The sample with Actilox and TAHHT-DDPO (Figure 18c) shows a continuous char surface correlating to V0 rating in UL94. Particularly for the Actilox and TAHHT-DOPO containing sample (Figure 18b), spherical particles with a diameter of about 50 μm can be observed. The residue of small Actilox particles (1.8 μm diameter) acts as initial nuclei for crystallization. This is also observed in the TG measurements under synthetic air discussed in Section 3.3.1 by the second decomposition step that is more distinctive for Actilox than for Disperal (35 μm diameter). This is an additional flame-retardant activity in the condensed phase at temperatures above 400 $^{\circ}\text{C}$, but the amount of phosphorus-containing synergist is not sufficient for a UL94 V0 rating. Literature [31] showed for ATH in unsaturated polyester resins that crystalline particles with a smaller specific surface area and phosphorus species with a hydrogen/carbon rich environment show gas-phase activity as well as the formation of a dense and tough residue, whereas the use of amorphous particles with a bigger specific surface area formed a fragile residue. This observation corresponds to this work, as Actilox has a BET-surface of 3 $\text{m}^2\cdot\text{g}^{-1}$ and Disperal a BET surface of 100 $\text{m}^2\cdot\text{g}^{-1}$.

4. Conclusions

The successful synthesis of novel phosphorus-containing polyacrylamides allows different applications. The synthesis itself is simple, versatile, and combines phosphorus and nitrogen in polymeric flame retardants. The selection of phosphorus species and multifunctional acrylamides as well as the ratio of the components is open. Different product properties like thermal stability or predominant flame retardant mechanism can be designed. Thermoset or thermoplastic polymers can be synthesized. In particular, the thermoplastics are soluble in epoxy resins and suitable for injection-molding processes.

This research deals with the polymeric phosphorus containing flame retardants BA-DOPO, TAHHT-DOPO, TAHHT-DDPO and TAHHT-DOPO-DDPO. The thermal stability determined by TG measurements showed that DOPO combined with BA is decomposed at lower temperatures than DOPO combined with TAHHT. The flame-retardant efficiency was tested in neat RTM6 resin and in carbon fiber reinforced composite materials. A second focus was the retardation of the fiber degradation leading to respirable fiber fragments with diameters below 3 μm . While the gas phase active DOPO containing flame retardants showed the best flame retardant efficiency by decreasing pHRR, THR and MARHE and delaying tti in cone calorimetric measurements, TAHHT-DDPO showed the best fiber protection caused by the observed flame retardant activity in the condensed phase (char formation). In agreement with the fiber protection and flame retardancy, the mixed polyacrylamide TAHHT-DOPO-DDPO is the most efficient. In conclusion, by incorporation of any investigated phosphorus-containing flame retardant in amounts of 10% by matrix weight, the fiber degradation can be retarded sufficiently as no respirable fiber fragments and no formation of defects on the fiber surface were observed by SEM. No relation of surface temperature during combustion and fiber degradation was found. The effect of fiber protection is a result of a loose residue on the fibers and between the laminates as shown by EDX measurements. Since the polarity of the formed phosphate does not fit carbon fibers, the aim to create a continuous protection layer on the fiber surface still has to be pursued. The use of the flame-retarded RTM6 in high-performance composites is still possible since interlaminar shear strength, T_g and hot-wet properties were not affected significantly by the incorporation of these flame retardants.

Additional investigations with boehmite containing RTM6 samples showed the possible use of the phosphorus containing polyacrylamides as synergist with inorganic fillers. Especially the formulation of RTM6 with TAHHT-DDPO and Actilox B30 showed a continuous residue surface which explains the V0 classification in UL94 tests. The particles of Actilox B30 have a smaller specific surface area than the particles of Disperal 40 and act as nuclei for the formation of a continuous char layer, providing an additional activity in the condensed phase at temperatures above 400 $^{\circ}\text{C}$. In particular,

the residue of the RTM6 formulation with Actilox B30 and TAHHT-DOPO showed spherical particles after combustion.

Author Contributions: L.G., M.D. and S.E. designed the experiments; L.G. and P.K. performed the experiments; L.G. analyzed the data; L.G. wrote the overall paper with P.K. contributing part 3.3.

Funding: The APC was funded by Röchling Stiftung GmbH.

Acknowledgments: The authors would like to thank the Röchling Stiftung GmbH for the financial support.

Conflicts of Interest: The authors declare no conflict of interest. The funders had no role in the design of the study; in the collection, analyses, or interpretation of data; in the writing of the manuscript, or in the decision to publish the results.

References

1. Zang, L.; Wagner, S.; Ciesielski, M.; Müller, P.; Döring, M. Novel star-shaped and hyperbranched phosphorus-containing flame retardants in epoxy resins. *Polym. Adv. Technol.* **2011**, *22*, 1182–1191. [[CrossRef](#)]
2. Perret, B.; Schartel, B.; Stöß, K.; Ciesielski, M.; Diederichs, J.; Döring, M.; Krämer, J.; Altstädt, V. A New Halogen-Free Flame Retardant Based on 9,10-Dihydro-9-oxa-10-phosphaphenanthrene-10-oxide for Epoxy Resins and their Carbon Fiber Composites for the Automotive and Aviation Industries. *Macromol. Mater. Eng.* **2011**, *296*, 14–30. [[CrossRef](#)]
3. Döring, M.; Ciesielski, M.; Heinzmann, C. Synergistic flame retardant mixtures in epoxy resins. In *Fire and Polymers VI: New advances in flame retardant chemistry and science*; Morgan, A.B., Wilkie, C.A., Nelson, G.N., Eds.; American Chemical Society: Washington, DC, USA, 2012; Volume 1118, pp. 295–309.
4. Ciesielski, M.; Diederichs, J.; Döring, M.; Schäfer, A. Advanced flame retardant epoxy resins for composite materials. In *Fire and Polymers V: Materials and Concepts for Fire Retardancy*; Wilkie, C.A., Morgan, A.B., Nelson, G.L., Eds.; American Chemical Society: Washington, DC, USA, 2009; Volume 1013, pp. 174–190.
5. Levchik, S.V.; Camino, G.; Costa, L.; Luda, M.P. Mechanistic study of thermal behaviour and combustion performance of carbon fibre-epoxy resin composites fire retarded with a phosphorous-based curing system. *Polym. Degrad. Stab.* **1996**, *54*, 317–322. [[CrossRef](#)]
6. Martin, F.J.; Price, K.R. Flammability of epoxy resins. *J. Appl. Polym. Sci.* **1968**, *12*, 143–158. [[CrossRef](#)]
7. Toldy, A.; Szolnoki, B.; Marosi, G. Flame retardancy of fibre-reinforced epoxy resin composites for aerospace applications. *Polym. Degrad. Stab.* **2011**, *96*, 371–376. [[CrossRef](#)]
8. Rabe, S.; Chuenban, Y.; Schartel, B. Exploring the Modes of Action of Phosphorus-Based Flame Retardants in Polymeric Systems. *Materials* **2017**, *10*, 455. [[CrossRef](#)]
9. Schartel, B.; Perret, B.; Dittrich, B.; Ciesielski, M.; Krämer, J.; Müller, P.; Altstädt, V.; Zang, L.; Döring, M. Flame retardancy of polymers: The role of specific reactions in the condensed phase. *Macromol. Mater. Eng.* **2016**, *301*, 9–35. [[CrossRef](#)]
10. Schartel, B. Phosphorus-based flame retardancy mechanisms-old hat or a starting point for future development? *Materials* **2010**, *3*, 4710–4745. [[CrossRef](#)]
11. Eibl, S.; Reiner, D.; Lehnert, M. Gefährdung durch lungengängige Faserfragmente nach dem Abbrand Kohlenstofffaser verstärkter Kunststoffe (Health hazards by respirable fiber fragments after combustion of carbon fiber reinforced plastic material). *Gefahrstoffe - Reinhaltung der Luft* **2014**, *74*, 286.
12. Eibl, S.; Scholz, N. Besondere Gefährdung beim Abbrand von Carbon-Kunststoffen (Particular hazards related to combustion of carbon fiber reinforced plastic material). *Brandschutz, Deutsche Feuerwehr-Zeitung* **2014**, *6*, 423–427.
13. Hertzberg, T. Dangers relating to fires in carbon-fibre based composite material. *Fire Mater.* **2005**, *29*, 231–248. [[CrossRef](#)]
14. Holt, P.F.; Horne, M. Dust from Carbon Fibre. *Environ. Res.* **1978**, *17*, 276–283. [[CrossRef](#)]
15. Eibl, S. Potential for the formation of respirable fibers in carbon fiber reinforced plastic materials after combustion. *Fire Mater.* **2017**, *41*, 808–816. [[CrossRef](#)]
16. World Health Organization (WHO). *Hazard Prevention and Control in the Work Environment: Airborne Dust*, WHO/SDE/OEH/99.14; 1999; Available online: http://www.who.int/occupational_health/publications/en/oehairbornedust3.pdf (accessed on 18 December 2017).
17. Eibl, S. Flammgeschützte Kohlenstofffaser (Flame retardant carbon fiber). DE 102015010001 A1, 2 February 2017.

18. Braun, U.; Balabanovich, A.I.; Schartel, B.; Knoll, U.; Artner, J.; Ciesielski, M.; Döring, M.; Perez, R.; Sandler, J.K.; Altstädt, V.; et al. Influence of the oxidation state of phosphorus on the decomposition and fire behaviour of flame-retarded epoxy resin composites. *Polymer* **2006**, *47*, 8495–8508. [[CrossRef](#)]
19. Pawlowski, K.H.; Schartel, B. Flame retardancy mechanisms of triphenyl phosphate, resorcinol bis(diphenyl phosphate) and bisphenol A bis(diphenyl phosphate) in polycarbonate/acrylonitrile-butadiene-styrene blends. *Polym. Int.* **2007**, *56*, 1404–1414. [[CrossRef](#)]
20. Wang, X.; Hu, Y.; Song, L.; Xing, W.; Lu, H.; Lv, P.; Jie, G. Flame retardancy and thermal degradation mechanism of epoxy resin composites based on a DOPO substituted organophosphorus oligomer. *Polymer* **2010**, *51*, 2435–2445. [[CrossRef](#)]
21. Moy, P.Y.; Gregor, A.I.; Pirelli, R.L.; Bright, D.A. Oligomeric Bis-Phosphate Flame Retardants and Compositions Containing The Same. EP2089402 B1, 19 August 2009.
22. Hamciuc, C.; Vlad-Bubulac, T.; Serbezeanu, D.; Carja, I.-D.; Hamciuc, E.; Lisa, G.; Pérez, V.F. Environmentally friendly fire-resistant epoxy resins based on a new oligophosphonate with high flame retardant efficiency. *RSC Adv.* **2016**, *6*, 22764–22776. [[CrossRef](#)]
23. Wang, X.; Hu, Y.; Song, L.; Yang, H.; Xing, W.; Lu, H. Synthesis and characterization of a DOPO-substituted organophosphorus oligomer and its application in flame retardant epoxy resins. *Prog. Org. Coat.* **2011**, *71*, 72–82. [[CrossRef](#)]
24. Perret, B.; Schartel, B.; Stöß, K.; Ciesielski, M.; Diederichs, J.; Döring, M.; Krämer, J.; Altstädt, V. Novel DOPO-based flame retardants in high-performance carbon fibre epoxy composites for aviation. *Eur. Polym. J.* **2011**, *47*, 1081–1089. [[CrossRef](#)]
25. Müller, P.; Bykov, Y.; Döring, M. New star-shaped phosphorus-containing flame retardants based on acrylates for epoxy resins. *Polym. Adv. Technol.* **2013**, *24*, 834–840. [[CrossRef](#)]
26. Minegishi, S.; Komatsu, S.; Kameyama, A.; Nishikubo, T. Novel synthesis of polyphosphonates by the polyaddition of bis(epoxide) with diaryl phosphonates. *J. Polym. Sci., Polym. Chem. Ed.* **1999**, *37*, 959–965. [[CrossRef](#)]
27. Ye, X.; Wang, Y.; Zhao, Z.; Yan, H. A novel hyperbranched poly(phosphorodiamidate) with high expansion degree and carbonization efficiency used for improving flame retardancy of APP/PP composites. *Polym. Degrad. Stab.* **2017**, *142*, 29–41. [[CrossRef](#)]
28. El Gouri, M.; El Bachiri, A.; Hegazi, S.E.; Rafik, M.; El Harfi, A. Thermal degradation of a reactive flame retardant based on cyclotriphosphazene and its blend with DGEBA epoxy resin. *Polym. Degrad. Stab.* **2009**, *94*, 2101–2106. [[CrossRef](#)]
29. Pagliuca, A. Flame Retardant Material and a Cable Having a Cable Sheath Composed of the Same. US 2011/0269888 A1, 3 November 2011.
30. Sun, T.; Zhuo, Q.; Chen, Y.; Wu, Z. Synthesis of boehmite and its effect on flame retardancy of epoxy resin. *High Perform. Polym.* **2014**, *27*, 100–104. [[CrossRef](#)]
31. Reuter, J.; Greiner, L.; Schönberger, F.; Döring, M. Synergistic flame retardant interplay of phosphorus containing flame retardants with aluminum trihydrate depending on the specific surface area in unsaturated polyester resin. *J. Appl. Polym. Sci.* **2019**, *136*, 47270. [[CrossRef](#)]
32. Hexcel Inc. Product data sheet RTM6. Available online: www.hexcel.com (accessed on 24 December 2018).
33. Schuster, T.J.; Eibl, S.; Gudladt, H.-J. Influence of carbon nanotubes on thermal response and reaction to fire properties of carbon fibre-reinforced plastic material. *J. Compos. Mater.* **2017**, *52*, 567–579. [[CrossRef](#)]
34. *Prüfungen zur Beurteilung der Brandgefahr - Teil 11-10: Prüfflammen - Prüfverfahren mit einer 50-W-Prüfflamme horizontal und vertikal (IEC 60695-11-10:2013)*, 2015; DIN EN 60695-11-10.
35. Babrauskas, V. Development of the cone calorimeter—A bench-scale heat release rate apparatus based on oxygen consumption. *Fire Mater.* **1984**, *8*, 81–95. [[CrossRef](#)]
36. *Reaction-to-fire Tests—Heat release, Smoke Production and Mass Loss Rate*; ISO: Geneva, Switzerland, 2002; ISO 5660-1,2.
37. Schartel, B.; Hull, T.R. Development of fire-retarded materials—Interpretation of cone calorimeter data. *Fire Mater.* **2007**, *31*, 327–354. [[CrossRef](#)]
38. *Aerospace series—carbon fiber reinforced plastics—unidirectional laminates; determination of apparent interlaminar shear strength*, 1997; DIN EN 2563:1997-03.
39. Weil, E.D.; Zhu, W.; Patel, N.; Mukhopadhyay, S.M. A systems approach to flame retardancy and comments on modes of action. *Polym. Degrad. Stab.* **1996**, *54*, 125–136. [[CrossRef](#)]

40. Petreus, O.; Popescu, F.N.; Cascaval, C.N. Action of some organophosphonic compounds on a diglycidyl ether-bisphenol-A epoxy resin. *Die Angewandte Makromolekulare Chemie* **1994**, *222*, 13–23. [[CrossRef](#)]
41. Rose, N.; Le Bras, M.; Delobel, R.; Costes, B.; Henry, Y. Thermal oxidative degradation of an epoxy resin. *Polym. Degrad. Stab.* **1993**, *42*, 307–316. [[CrossRef](#)]
42. Rose, N.; Le Bras, M.; Bourbigot, S.; Delobel, R. Thermal oxidative degradation of epoxy resins: evaluation of their heat resistance using invariant kinetic parameters. *Polym. Degrad. Stab.* **1994**, *45*, 387–397. [[CrossRef](#)]
43. Nabaltec AG. *Actilox Boehmite Product Data Sheet*. Available online: https://nabaltec.de/fileadmin/user_upload/03_produkte/03-3_boehmit/nabaltec_tds_actilox-as1.pdf (accessed on 5 February 2019).
44. Sasol GmbH. *DISPERAL/DISPAL Product Data Sheet*. Available online: www.sasoltechdata.com/tds/DISPERAL_DISPAL.pdf (accessed on 5 February 2019).



© 2019 by the authors. Licensee MDPI, Basel, Switzerland. This article is an open access article distributed under the terms and conditions of the Creative Commons Attribution (CC BY) license (<http://creativecommons.org/licenses/by/4.0/>).